EXPERIMENTAL STUDY OF IGNITION OF MAGNESIUM POWDER BY ELECTRO-STATIC DISCHARGE

Authors:

Ervin Beloni and Edward L. Dreizin

ABSTRACT

Ignition sensitivity of powders to electro-static discharge (ESD) stimulation is commonly tested to assess the safety of powder handling. However, the mechanisms of powder ignition by electric spark remain unclear. This paper represents an experimental study in which the spark parameters are quantified and the ESD ignition of a metal powder is investigated. A spherical powder of Mg, for which thermal ignition kinetics was described in the literature, was used in experiments. The experimental setup was built based on a commercially available apparatus for ESD ignition sensitivity testing. Additional diagnostics enabled measurements of electrical current, voltage, and spark and ignited powder emission in real time. The spark duration was of the order of a few μs. The spark current and voltage were always observed to have significant AC components. The electrical impedance of the spark discharge was determined experimentally using the recorded current traces and assuming that the spark could be represented as a series LRC circuit. The optical emission was filtered to separate the signals produced by the spark plasma and by the heated and igniting powder. The radiation signal produced by the igniting powder was always delayed after the spark. The delay time decreased from about 3.5 to 0.5 ms as the spark energy increased from 10 to 60 mJ; the delay remained nearly constant when the spark energy continued to increase to over 100 mJ. For experiments where the powder volume decreased or where binder was introduced delay times were reduced, particularly above 60 mJ the delay time went down to 0 ms.

INTRODUCTION

Electro-static spark is a common ignition stimulus and a variety of tests, standards, and evaluation methodologies are developed to investigate ignition behavior of different substances struck by a spark. Electro-static discharge (ESD) ignition for flammable gases was studied in great detail and a number of important trends were established. Effects of electrode materials, electrode shape, discharge duration, and other similar parameters have been quantified and reported. Reviews by Mellor et al., [1-2] published in 1990's described these trends and suggested that a similar systematic study would be necessary to establish a scientifically sound test of ESD sensitivity of powders. However, such a study has never been undertaken. Note that ignition of various aerosolized powders has been studied by many investigators, e.g., [3-5]. However, the mechanisms of flame propagation in aerosols are different from those of non-aerosolized powders routinely tested in industry. In fact, an experimental test of ESD ignition sensitivity for non-aerosolized powders is one of the most commonly used to evaluate a

variety of powdered materials, including agricultural [6], food [7], textile [8], pharmaceutical [9], metallic [10-12], and of course, energetic components [13-14]. Typically, a spark is generated by a high-voltage capacitor discharging over a gap between a sharpened electrode and a powder bed. The minimum capacitor energy at which the powder ignites is specified as the minimum ignition energy (MIE), a parameter defining the sensitivity of a powder to ESD ignition stimulation. It has been suggested in ref. [14] that the spark represents primarily a thermal source capable of raising the temperature of a flammable powder above the point at which thermal runaway occurs. However, it remains unclear how the spark heats the powder particles, what portion of the spark energy is being transferred to the powder and by which mechanism. For example, the spark's plasma can heat the powder surface directly while the current of the spark discharge can result in Joule heating distributed in the powder volume, along the current path. It remains unclear whether the polarity of the spark discharge is a factor affecting the ignition energy. The transport properties of powders including their thermal and electrical conductivities are initially governed by the respective contact resistances between the particles. While a powder is heated, gasified, and/or being melted, its transport properties are expected to change dramatically [15-16] affecting its interaction with the spark. The spark itself does not behave as a steady heat source and the energy distribution is expected to change as a function of both time and location. However, it is unclear whether the ignition governed by a runaway chemical reaction occurs within the same time frame as the relatively short-lived spark discharge, and thus whether the temporal changes in the spark energy distribution are significant in affecting the ignition sensitivity of various materials.

Understanding the mechanisms of the ESD ignition of powders becomes increasingly important with dramatic acceleration in recent research aimed to develop new powdered materials, including nanomaterials for a variety of applications. Current protocols used for ESD ignition sensitivity testing, e.g., described in various standards, e.g., [17-18] are not based on such understanding and the results are often inconsistent between different testers and inconclusive in nature. Furthermore, the current protocols are not suitable for a number of newly developed powders, which are not available in the quantities required for the standardized testing. At the same time, often the development of the new material manufacturing processes necessary to produce sufficient material quantities may hinge upon its positive safety evaluation, of which a conclusive ESD sensitivity evaluation is a necessary part.

The goal of this work is to initiate a systematic study of the mechanisms of ESD powder ignition. The overall study is viewed as a combination of systematic experimental and modeling efforts ultimately resulting in quantitative mechanisms describing ignition of various powder-like materials by electric sparks. This paper represents the first part of this study and reports an experimental investigation of ESD ignition of a spherical metal powder. The paper describes measurements of optical emission produced by the spark and ignited powder and the spark current and voltage measurements. Magnesium was selected for this study because there are relatively reliable descriptions for its thermal ignition available in the literature [19-20]. Thus, it is expected that the results of the measurements reported in this paper would be useful for quantitative modeling of the ESD stimulated powder ignition in which the thermal runaway reaction in the powder is described with reasonable accuracy.

EXPERIMENTAL

Powder

The powder used in the ignition experiments was 1-11 μm spherical Mg by Hart Metals, Inc. The particle size distribution was measured using a Beckman-Coulter LS230 Enhanced Particle Analyzer. Based on the volumetric size distribution, the mean particle size was 10.3 μm. This same powder was earlier used in experiments on thermal ignition of Mg using an electrically heated filament [20] so that direct comparisons between some of the results presented in ref. [20] and in this paper are possible.

Electrostatic discharge apparatus

A schematic diagram of the experimental setup is shown in Fig. 1. A Model 931 Firing Test System (FTS) by Electro-Tech Systems, Inc. was used to generate spark discharges. FTS includes a capacitor bank with capacitance varied in the range of 100 – 10000 pF. The capacitors can be discharged through the spark gap directly or through an additional resistor varied from 500 to 5000 Ω. Additional resistors were not used in this project. The capacitors can be charged to a voltage varied from 100 V to 26 kV.

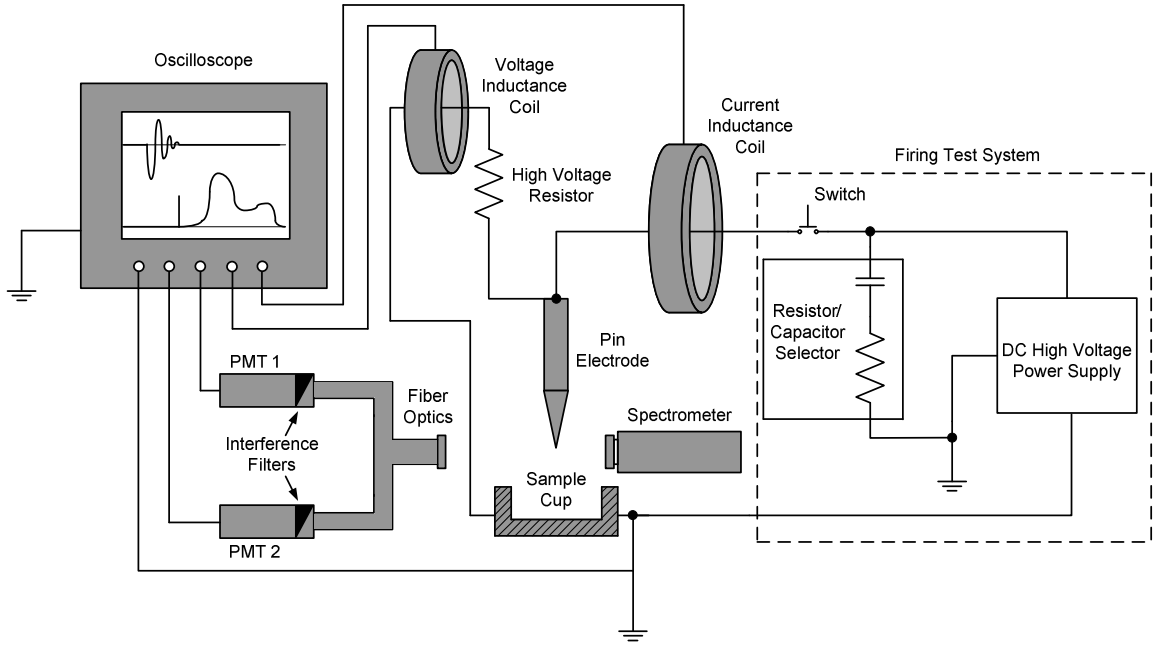

Figure 1. Schematic diagram of the experimental setup.

The polarity of the electric output can be changed so that the high-voltage electrode can be either positive or negative. For a standard test [17], the powder is placed into a stainless steel cup (15 mm diameter, 3 mm deep) affixed to a grounded base. The high voltage pin-electrode (a stainless steel needle) is placed 0.2 mm above the surface of the powder being tested. If sufficient energy is delivered to the powder, ignition occurs. In a

standard test [17], ignition is determined to have occurred when the ignited powder produces a bright white flame.

Sample holders

Three sample holders were used in this study. A standard sample holder is a stainless steel cup described above. In addition, two custom-made sample holders were made and used to assess the effect of the powder amount on its ignition. For both custom-made sample holders, it was desired to avoid the possibility for the spark to strike the sample holder surface rather than the powder directly. Therefore, the only conductive surfaces of each of the two customized sample holders were their bottom surfaces on which the powder was placed. The sample holders comprised aluminum plates with dielectric washers affixed by an epoxy resin. A 6 mm internal diameter, 0.5 mm-thick nylon washer was used to make a larger customized sample holder. Similarly, a 2.1 mm internal diameter, 0.6 mm-thick polycarbonate washer was used to make a smaller sample holder.

Binder

Several experiments were conducted with a small amount of binder added to Mg powder in order to investigate the effect of powder ejection by electric spark (see below) on its ignition. The binder chosen for these experiments was Star Brite liquid electrical tape which contains a vinyl acetate co-polymer, hydrocarbons, and ketones [21]. 0.1 g of binder was diluted in 10 mL of acetone. 1 mL of the diluted binder solution was added to 0.4 g of powder, thoroughly mixed, added to the sample holder, and air dried prior to testing. The binder amount was estimated to be only 0.3 wt. % of the binder/powder mixture. The binder was only used in selected tests utilizing a larger (6 mm diameter) customized sample holder described above.

Diagnostics

Inductance coils by Pearson Electronics were used to measure spark current and voltage across the pin electrode and sample gap. The current was measured using a model 110A coil with a 1 V / 10 A ratio. To measure the voltage drop, a 1 kΩ high voltage resistor was connected in parallel between the discharge pin and sample cup substrate. The current through the resistor proportional to the spark voltage was measured using a model 4100 coil with a 1 V / 1 A ratio. Both current and voltage traces were visualized and recorded by a LeCroy WaveSurfer 64Xs Series oscilloscope.

Optical emission produced by the spark and by the igniting powder was monitored in real time. In preliminary measurements, optical spectra produced respectively by sparks between the pin electrode and an empty sample cup and between the pin electrode and igniting Mg powder were recorded using an EPP2000 spectrometer by Stellarnet Inc. The recorded spectra are shown in Fig. 2 without correction for sensitivity of the spectrometer. The lack of correction results in a distortion of the black-body emission envelope, while the uncorrected spectra are still helpful for identifying the spectral regions most suitable for monitoring the emissions produced by the spark and by the

heated and ignited powder. The emission of the spark itself (generated over an empty sample cup) was dominated by an ultraviolet peak (around 280 nm).

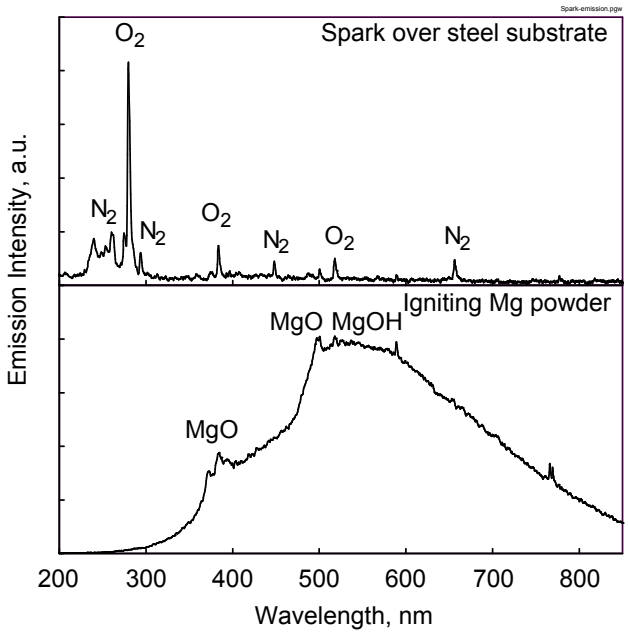

Figure 2. Emission spectra of the sparks between the pin electrode and an empty steel sample cup (top) and between the pin electrode and igniting Mg powder (bottom).

Based on refs. [22- 23], it was assigned to molecular oxygen. The emission of the igniting Mg powder was heavily dominated by a broad black-body spectrum with one of the strong peaks observed around 500 nm, assigned to MgO. Respectively, interference filters at 280 nm and 500 nm were selected to separate between the radiation signatures of the spark and igniting powder. A bifurcated fiber optics cable with a single input window was used to split the optical signal between two outputs. Each output was connected to a respective interference filter and a photomultiplier.

Preliminary characterization of the spark

In initial experiments, emission and electrical current traces were acquired for sparks striking solid metal substrates. The distance between the pin electrode and the substrate surface was maintained at 0.2 mm. The spark polarity, the value of the discharging capacitor, and the material of the substrate varied while the initial voltage was fixed at V_0=5 kV. Figure 3 shows typical examples of the current trace and radiation traces recorded using ultra-violet (280 nm) and green (500 nm) interference filters. Both the current and 280-nm filtered traces showed a strong AC component. Note that change in the pre-set polarity of the spark discharge using the FTS polarity selection did not appreciably change the shapes of the recorded current traces. The oscillations in current corresponding to the repeated re-charging of the capacitor correlated with the oscillations in the filtered spark emission signal.

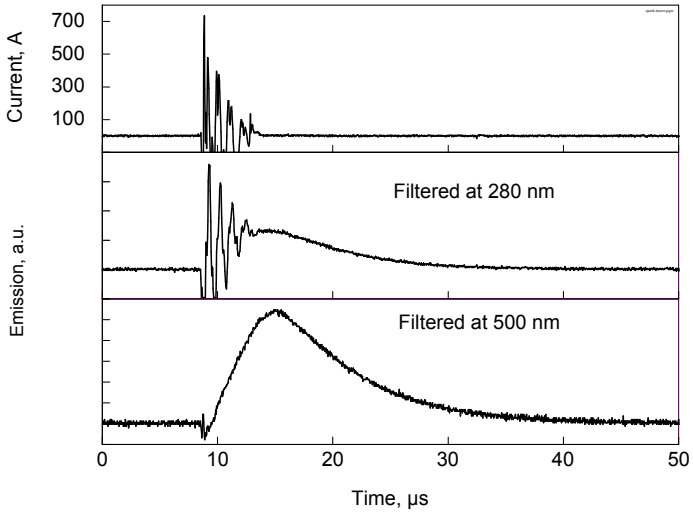

Figure 3. Examples of the spark current and emission traces (traces shown were obtained from a spark striking a stainless steel substrate, pin electrode was negative, V_0 = 5 kV, C = 5000 pF, and no additional resistor).

The green filtered trace showed no oscillations and the signal continuously increased during the time the spark current was measured. This clearly indicates the thermal radiation produced by the surface heated by the spark. Both radiation traces were observed to decay after the current trace was reduced to zero.

Varied parameters

Spark energy was changed by changes in both applied voltage and selected capacitor. Experiments were performed at both spark polarities. The spark gap was varied between 0.2 mm, recommended by the ESD ignition testing standard [17] and 1.5 mm. The other experimental conditions and parameters included use of different size sample holders and use of binder for the Mg powder.

RESULTS

Powder Ejection

Initial ignition tests showed that a portion of the powder placed in a sample cup is ejected from the cup for both ignition and non-ignition cases. A small crater, of about 1 – 3 mm diameter was always formed at the location where the spark struck the powder. Examples of the produced craters for the powder placed in the standard sample holder are shown in Fig. 4. The electrode cup on the left shows powder that has not been struck by a spark. The middle cup shows Mg powder that has been struck by a spark but did not ignite. A crater of about 3 mm diameter is clearly seen in the center of the cup. The cup on the right shows Mg powder that has been struck by a spark and the spark energy was sufficient to ignite the powder. A crater of about 3 mm diameter is again observed in the center of the cup. There is also a white oxide layer covering almost the entire powder

surface. It should be noted that the oxide layer formed after the spark was over while the powder away from the crater was burning for several seconds. Note that when the 6 mm diameter, custom sample holder was used the powder ejection and crater formation were observed, similar to the case illustrated in Fig. 4. For the smaller, 2.1 mm diameter sample holder, the ejection resulted in effective removal of the entire powder charge from the sample holder.

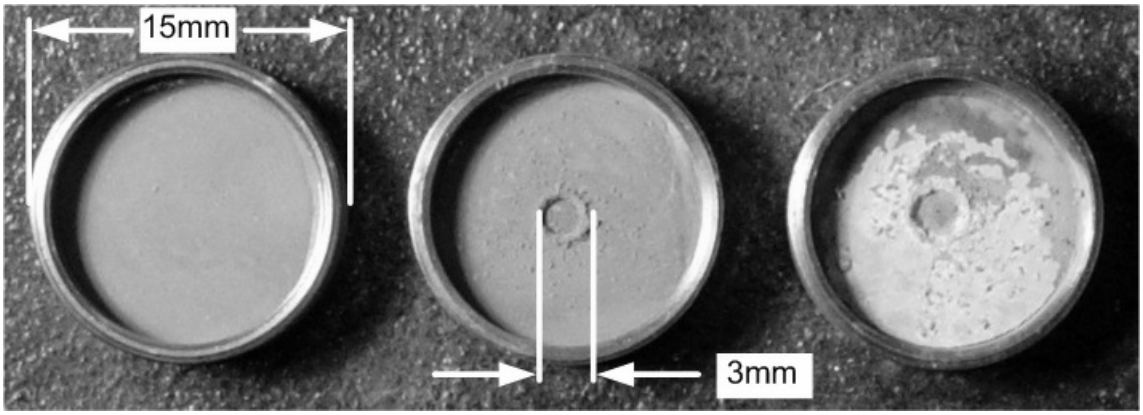

Figure 4. Electrode cups (15 mm diameter) containing Mg powder; left cup contains powder that has not been struck by a spark, middle cup contains powder that has been struck by a spark and has not ignited, and the right cup contains powder that has been struck by a spark and has ignited.

To determine the velocity of the ejected particles, the sample was illuminated using a modulated green laser sheet placed perpendicular to the powder sample holder. The spark energy was kept lower than the powder ignition threshold. Ejected, but not ignited particles scattered the laser light and were photographed using a digital camera with an open shutter. It was observed that the initial velocities at which the particles moved (measured about 1 mm from the powder surface) varied from 30 to 70 cm/s. The velocities were not affected by the spark voltage, systematically varied in these experiments.

The ejection of powder by the spark resulting in the formation of the central crater can be attributed to the effect of the spark-produced shock wave [24]. This shock wave passes through the powder layer, reflects from the bottom of the sample holder and the powder becomes accelerated and is lifted by the pressure produced in the reflected wave. The role of the powder ejection in the ignition mechanism has not been previously discussed in the literature.

Circuit impedance and measured spark energy

Current and voltage measurements were used to determine the total spark energy. In addition, the spark/powder impedance was roughly evaluated from processing the recorded current traces. The spark/powder system was assumed to be represented by an LRC series circuit, with constant values of resistance, R, inductance, L, and capacitance, C. Figure 5 shows typical experimental traces for the current and voltage. In addition, the best fit trace for the current signal is shown. The fit was obtained using the equation

of current for an LRC series circuit with no voltage source applied after the capacitor is charged to a specified voltage [25]:

$$I(t) = -\frac{2CV_A}{\sqrt{4LC - R^2C^2}} \cdot \sin\left(\sqrt{\frac{1}{LC} - \frac{R^2}{4L^2}}t + \theta\right) \cdot \exp\left(-\frac{R}{2L}t\right) \quad (1)$$

where *I(t)* is the spark current as a function of time, *t*; V_A is the voltage applied to charge the capacitor, and θ is the phase angle. The values of *L*, *R*, and *C* were adjusted to obtain the fit of the current trace predicted by Eq. (1) and the experimental trace. Note that in order to produce estimates meaningful for description of spark ignition events, it should be recognized that the assumption of the constant impedance made above to find the *L, R,* and *C* values by matching the experimental current trace and prediction using Eq. (1) cannot be entirely accurate.

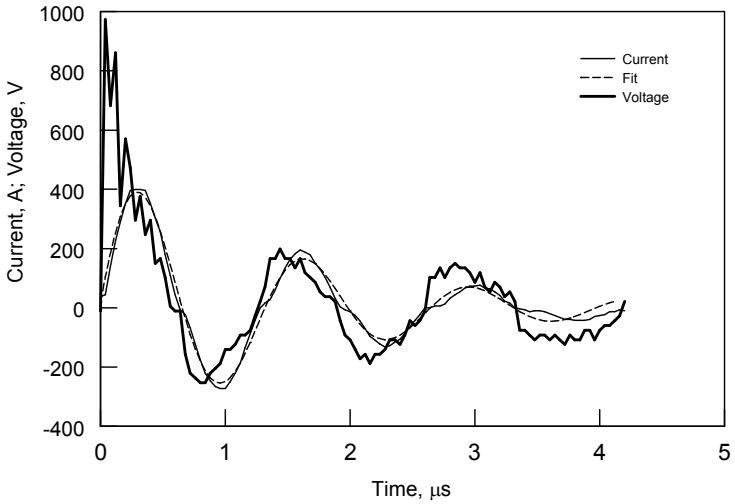

Figure 5. Experimental current and voltage traces for a spark and a current trace obtained fitting the experimental data and assuming the spark as a series LRC circuit.

The impedance of the spark/powder system is likely to change in time, both due to substantial changes in the conductivity of non-equilibrium plasma existing in the spark gap [26-27], and due to changes in the properties of Mg powder while it is being heated and melted. In initial analyses it was noticed that the quality of match between the experimental and calculated curves (as shown in Fig. 5) was consistently different for the earlier and later spark times. The earlier times play a greater role for the energy transfer from the spark to the powder, both because of the initially higher conductivity of the spark kernel [26-27] and because of the rapid decrease in the amplitude of the discharge current with time. Therefore, to obtain the current fitting curves and identify the values of *R, L,* and *C*, most useful for description of the energy transfer from the spark to powder, the experimental current trace was truncated as shown in Fig. 5 to remove two of the final and weakest oscillation periods observed. This resulted in a description matching better with the experimental current at the earlier times.

The spark energy was determined as:

$$E = \sum IV\Delta t \quad (2)$$

where the summation was performed over the entire spark duration with the time step Δt equal to the sampling time of the digital oscilloscope and using the recorded values of I and V as a function of time. For all current and voltage measurements the time step was Δt = 40 ns. Equation (2) estimates the true or active portion of the total released energy available for heating the conductive elements of the circuit. It does not include the reactive energy, which might result in some losses through electromagnetic radiation produced by the phase-shifted components of the current and voltage existing due to the inductive nature of the spark circuit impedance. Similar measurements were performed and processed for empty sample holders and for the sample holders with Mg powder. The results of this signal analysis and obtained values of the spark energy are shown in Figs. 6, 7. Each measurement here and below was repeated 10 times. The error bars show one standard deviation of the 10 repetitions.

The spark energy measured for empty sample holders under various experimental conditions is shown as a function of the energy stored in the capacitor in Fig. 6. Only about 1/6th of the capacitor's energy is recovered as determined from the recorded current and voltage traces and using Eq. (2).

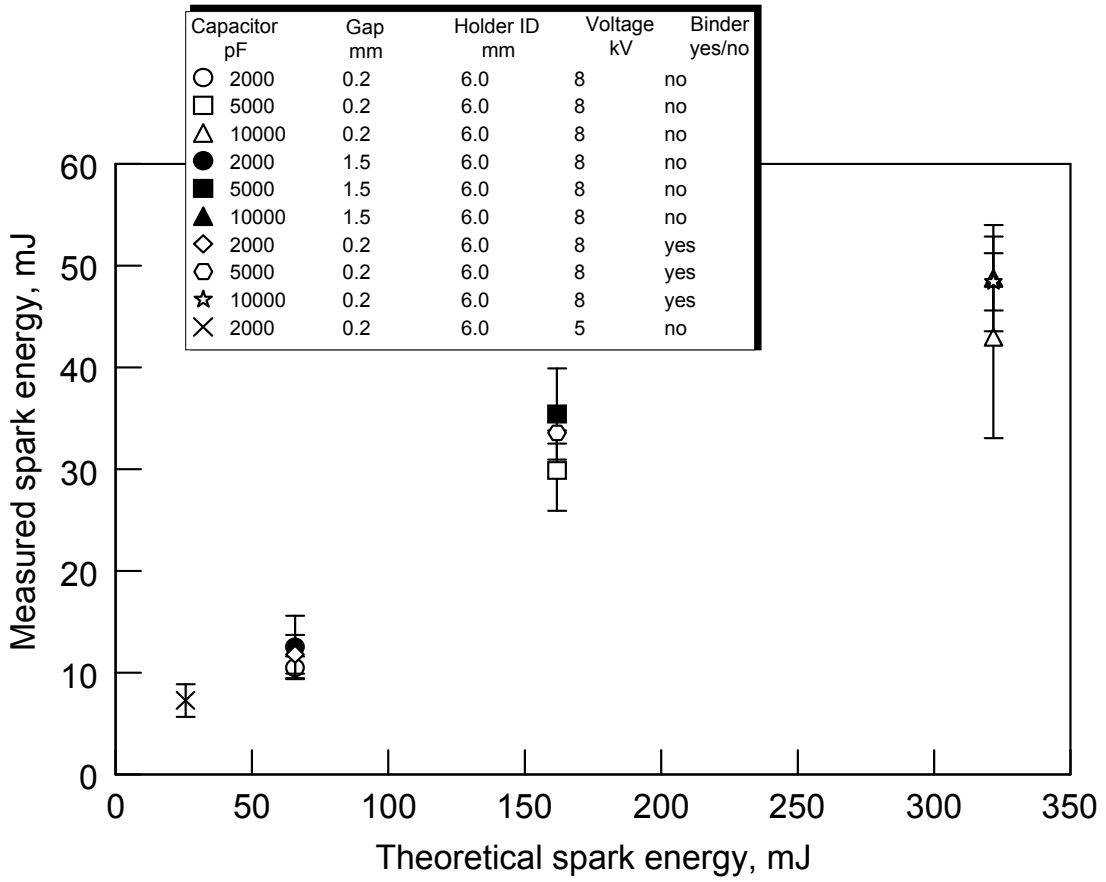

Figure 6. Measured active spark energy as a function of the energy stored in the capacitor for empty sample holders with different diameters and for different spark gaps and capacitor values.

A small part of the capacitor's energy is unaccounted for because of the truncated current trace. It is also possible that the capacitor retains some small charge after the spark discharge is over. Furthermore, it is hypothesized that a substantial part of the capacitor's energy is unaccounted for by Eq. (2) due to the inductive nature of the spark's impedance. Slightly higher measured spark energies correspond to the longer spark gap, while the effect is weak. No effect of the sample holder size can be detected. A similar plot for the spark energy measured for the sample holders filled with Mg powder as a function of the energy stored in the capacitor is shown in Fig. 7.

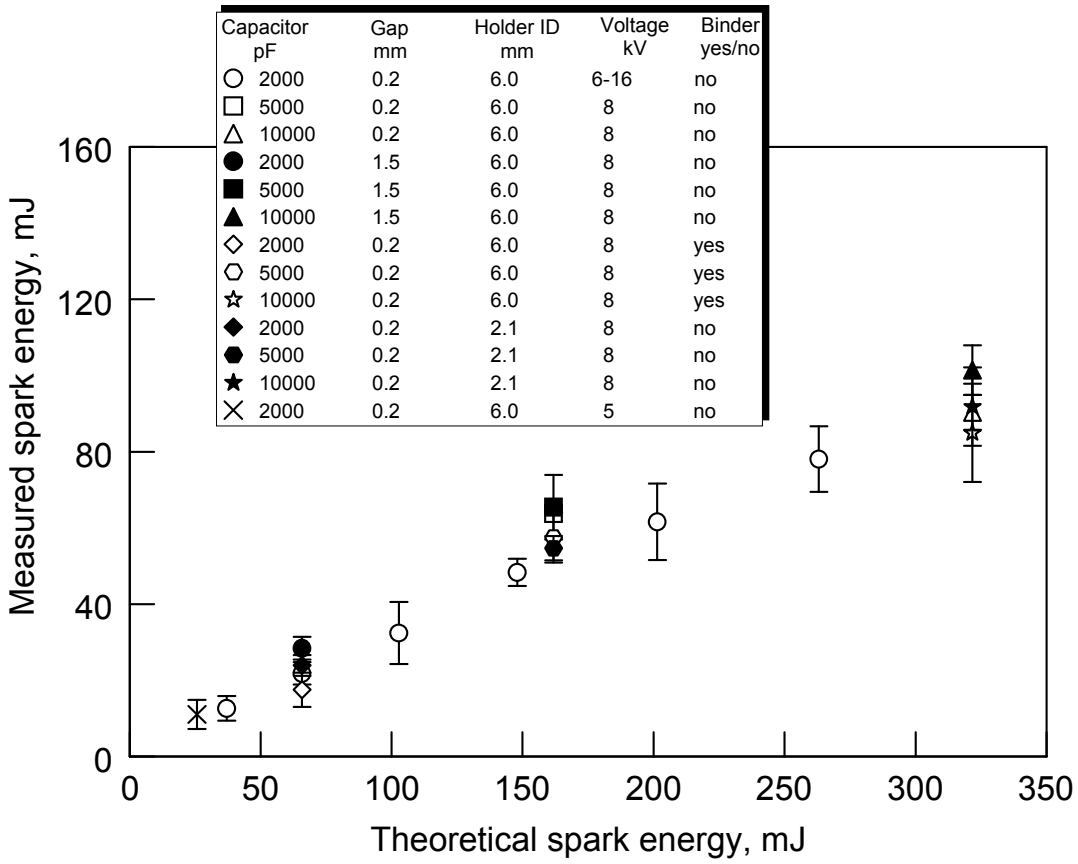

Figure 7. Measured active spark energy as a function of the energy stored in the capacitor for sample holders with different diameters filled with Mg powder with and without binder and for different spark gaps and capacitor values.

It is interesting that in the latter case, the measured spark energy is about 1/3rd of the capacitor's energy, or about two times greater than it is for the same experimental configuration but without Mg powder. This can be attributed to the added active resistance caused by the Mg powder. With this additional resistance, the overall spark impedance becomes less inductive, so that a greater portion of the capacitor's energy is recovered using the measured traces of *I* and *V* and Eq. (2).

The spark impedance values obtained from matching the current traces using the current description given by Eq. (1) are shown in Figs. 8 and 9. The *L, R, C* values corresponding to the empty sample holder are shown in Fig. 8. The capacitance shown is

a correction to the pre-set capacitance of the FTS required for the best fit for the measured current trace using Eq. (1). Clear trends of reduced resistance and inductance and increased capacitance at the higher spark energies are observed. The effect of the spark gap on the determined spark impedance is negligible.

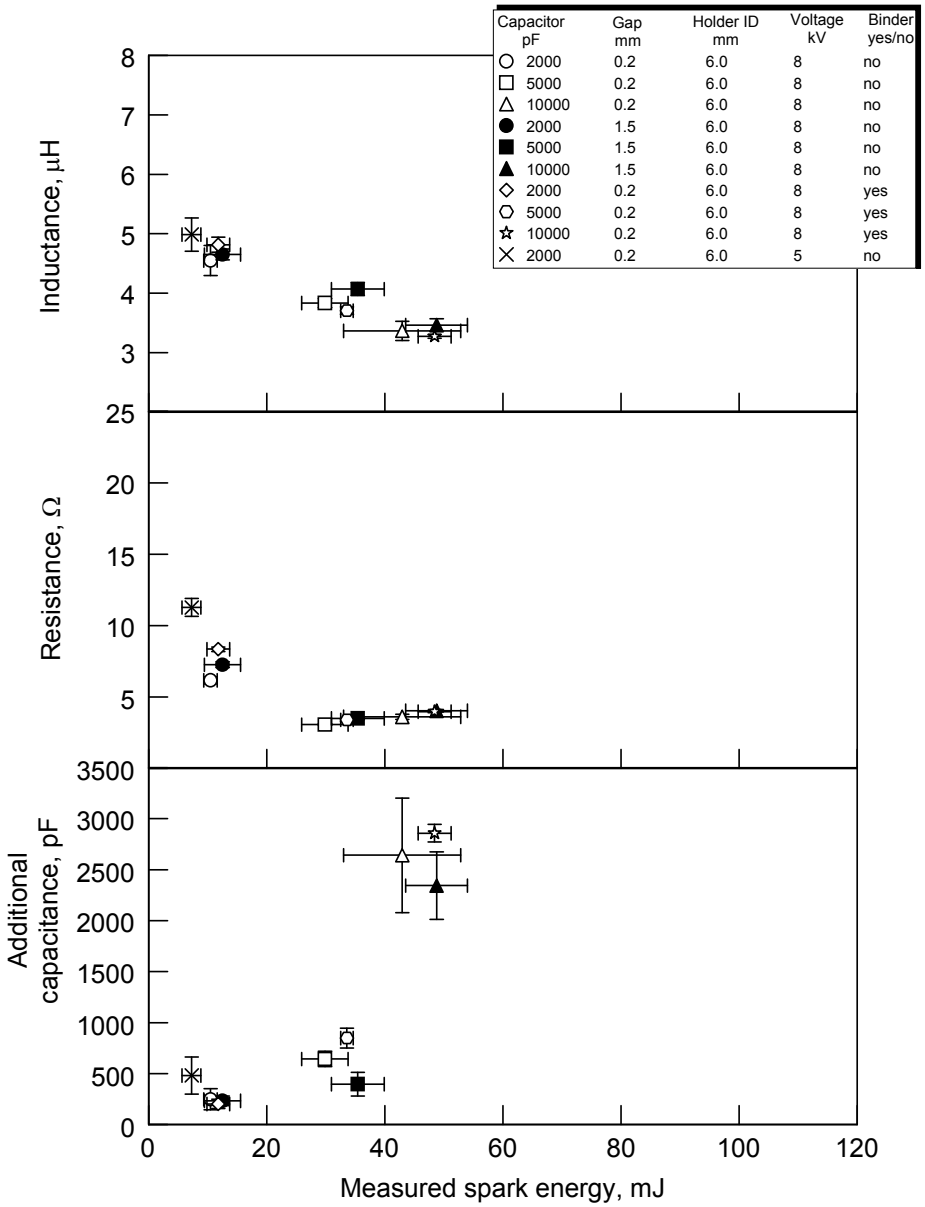

Figure 8. Circuit impedance as a function of the measured spark energy for the experiments with both the 6 mm diameter and 2.1 mm diameter empty sample holders (spark only).

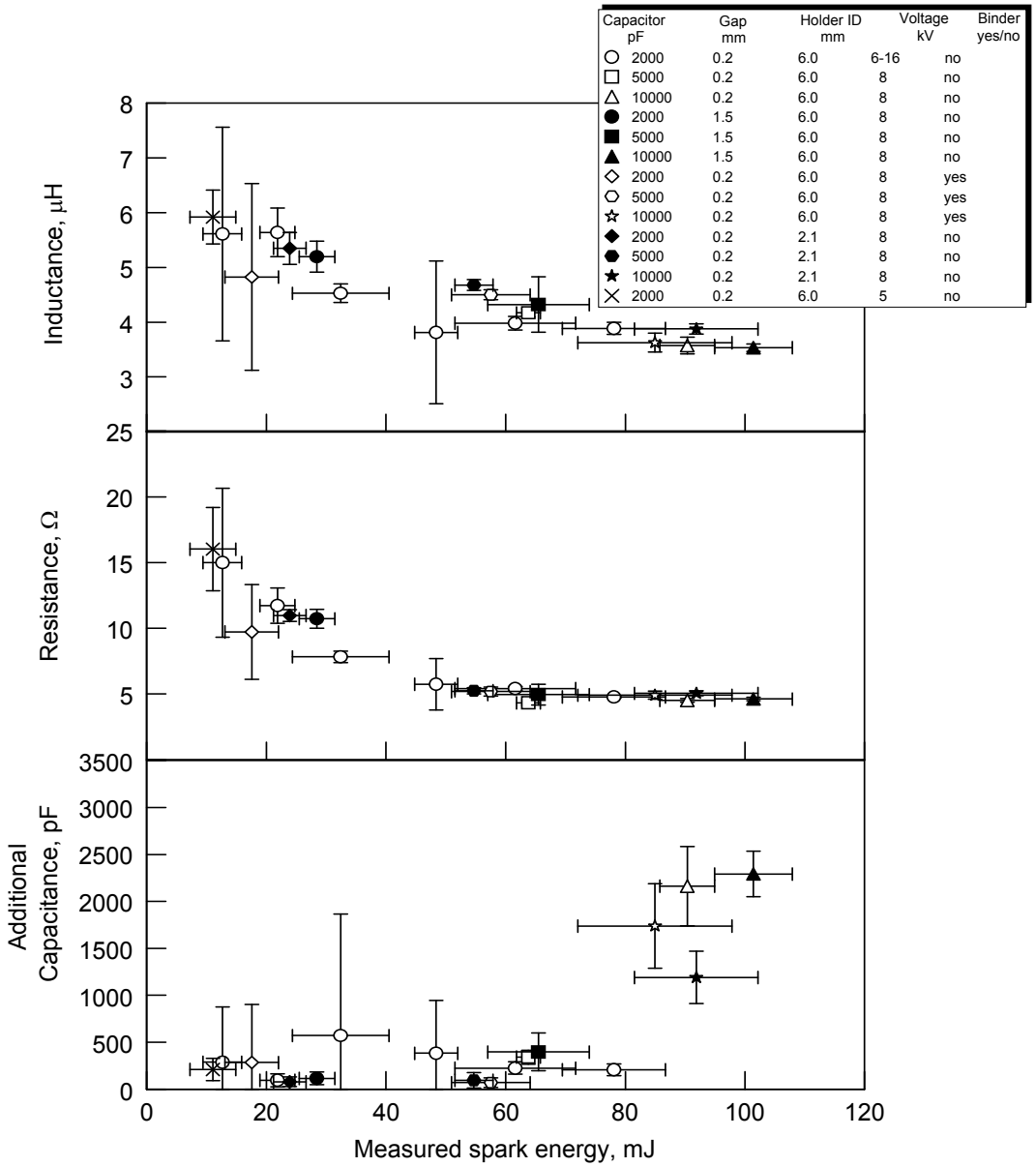

Figure 9. Circuit impedance as a function of the measured spark energy for the experiments with igniting loose Mg powder in 6 mm diameter sample holder, Mg with binder in a 6 mm diameter sample holder, and loose Mg in a 2.1 mm diameter sample holder.

For experiments with Mg powder, impedance values are shown in Fig 9. Results are shown for ignited Mg placed in both 2.1 and 6 mm diameter custom-made sample holders with the latter used with and without binder added to the powder. In addition, results obtained for measurements with different spark gap lengths are shown. It is observed that adding powder slightly increases the values of resistance and inductance necessary to fit the experimental data with the shape predicted by Eq. (1) for all spark energies. This is consistent with the observed greater portion of the capacitor's energy recovered as calculated by Eq. (2). There is no detectable effect of the spark gap or

binder on the resistance and inductance values. The trends of reduced inductance and resistance and increased capacitance with increased spark energies are clearly visible and similar to those observed from Fig. 8.

The correction for the capacitance value is relatively small for all, except for the largest used capacitor (10,000 pF), for which it reaches about 20% of the capacitor value. In most cases, the additional capacitance decreases with powder included. Binder addition and sample holder size do not have a clear affect on the additional capacitance.

Minimum Ignition Energy

The experiments using the standard sample holder and spark gap of 0.2 mm suggested by the standard procedure [17] established the minimum ignition energy for Mg powder to be 25 mJ. This value is the energy stored in the capacitor. The measured spark energy available to the powder is 11 mJ and the energy delivered from Joule heating is 5 mJ.

Ignition delays

It was observed that the optical signal produced by the ignited powder was noticeably delayed following the spark emission and current traces. The ignition delay is illustrated in Fig. 10. The top plot shows the initial (shaded) portion of the recorded signal with the logarithmic time scale, so that it is clearly observed that the emission decreases to its baseline level after the spark and the ignition peak is only detected after a substantial delay. The delay times were measured using the recorded emission traces. Two different signal processing techniques were used and respectively two different values of ignition delays were obtained for each of the recorded traces. In both cases, the baseline signal level was determined as the signal recorded prior to the spark ignition.

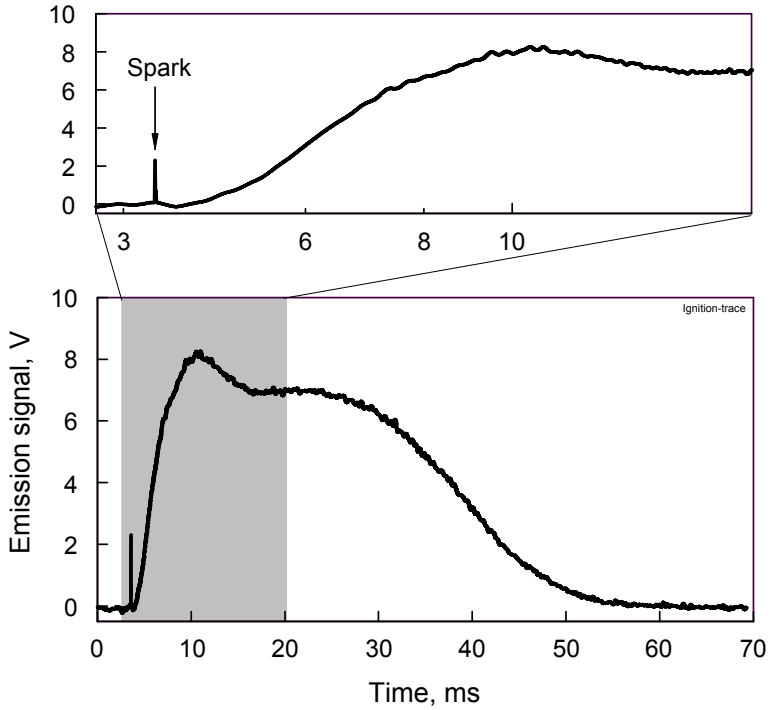

Figure 10. An emission signal produced by a spark-ignited Mg powder. A shaded portion of the signal is expanded with a logarithmic horizontal scale to clearly illustrate the short spark pulse soon after 3 ms preceding the Mg ignition that produces the main broad peak.

In the first moment considered to determine the ignition delay, the ignition was assumed to occur when the emission signal increased abruptly. Thus, the rate of ensuing combustion affecting the slope of the emission signal influenced the identification of the ignition moment. To find the delay by this method, a time derivative of the emission signal was obtained and the instant and signal value of the emission trace corresponding to the maximum in its derivative were found. The signal slope at this point was projected as a straight line to cross the baseline signal level, as illustrated in Fig. 11, so that the ignition delay could be determined.

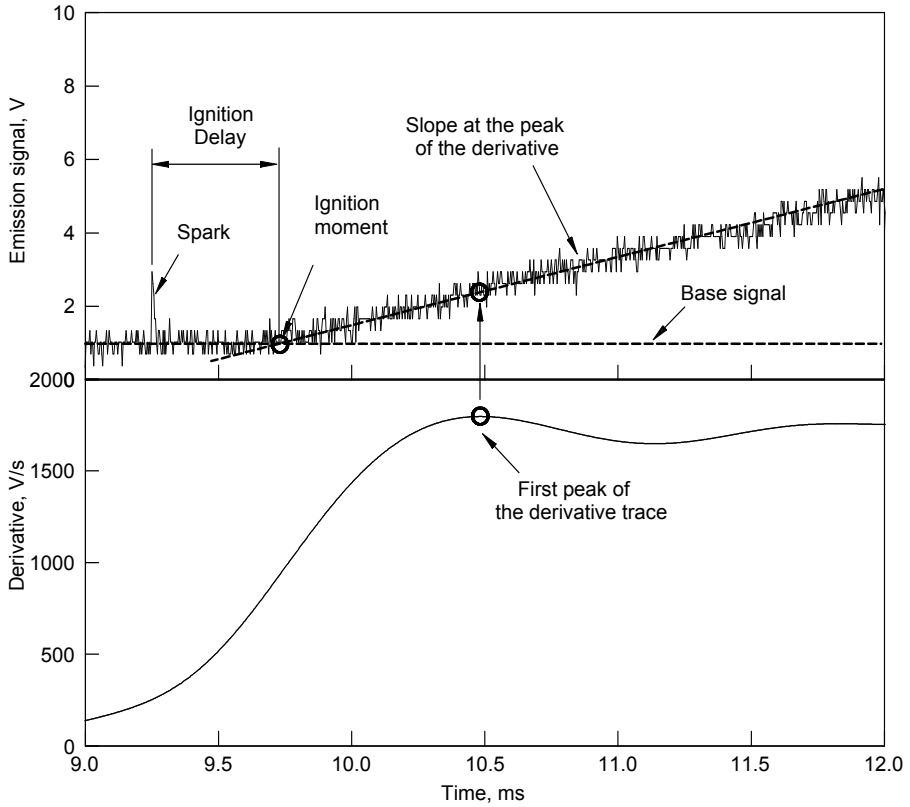

Figure 11. Illustration of the first method used to determine ignition delay. The bottom plot shows a derivative of the emission signal (the spark is not visible due to the signal smoothing). The top plot shows the respective portion of the recorded unprocessed signal and the identified slope corresponding to the first peak in its derivative. The time between the spark and the point where the slope line crosses the zero-level signal line is the measured delay.

In the second method, ignition was assumed to occur when the emission signal produced by the ignited powder exceeded the baseline signal. Specifically, the ignition instant chosen was when the emission signal following the spark increased 3 standard deviations above the baseline level, as illustrated in Fig. 12.

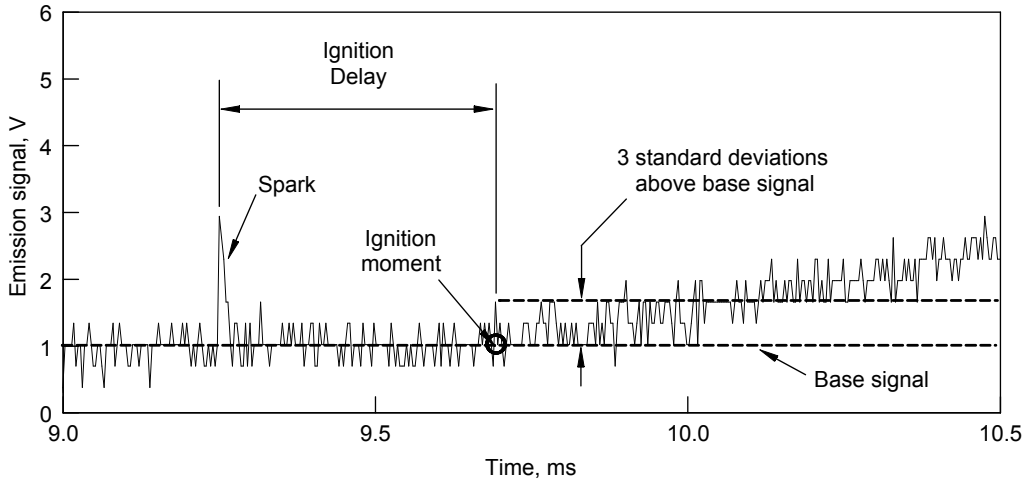

Figure 12. Illustration of the second method used to determine ignition delay. The ignition moment is chosen when the emission signal increases 3 standard deviations above the base signal noise after the spark.

Figures 13 – 14 show ignition delays versus measured spark energies for loose Mg powder in the 6 mm diameter sample holder where delays are determined by methods 1 and 2, respectively. Ignition delays vary in the range of 0.5 – 3 ms and correlate with the measured spark energy, with shorter delays corresponding to greater spark energies. This trend is also observed in experiments with Mg/binder in the 6 mm diameter sample holder and loose powder in the 2.1 mm diameter sample holder, as shown in Figs. 15 and 16, respectively. Results presented in Figs. 13 and 14 show no effect of the spark gap on ignition delay. Ignition delays are shorter in Figs. 15 – 16 as compared to Figs. 13 – 14 (loose powder on a 6 mm diameter sample holder). Interestingly, the effect of the spark energy on the ignition delay for experiments with binder is different from that for the loose powder. For the powder with binder, the ignition delay continues to decrease when the spark energy increases above 60 mJ (Fig. 16); at the same time the ignition delay becomes roughly constant above 60 mJ for the loose powder (Figs. 13 – 15). The specific value assigned to the ignition delay is affected by the method used for its quantification. According to Figs 15 – 16, method 2 yields shorter delays than method 1. However, according to Figs. 13 – 14, below 30 mJ method 2 yields shorter delays but above 30 mJ method 2 yields longer delays than method 1.

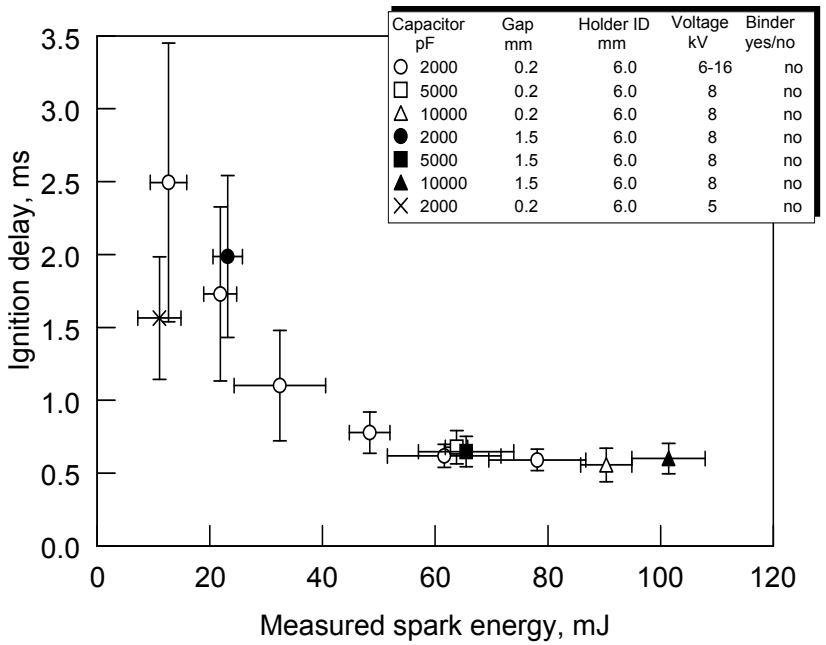

Figure 13. Ignition delay (method 1) v measured spark energy for experiments conducted with the 6 mm diameter sample holder and no binder.

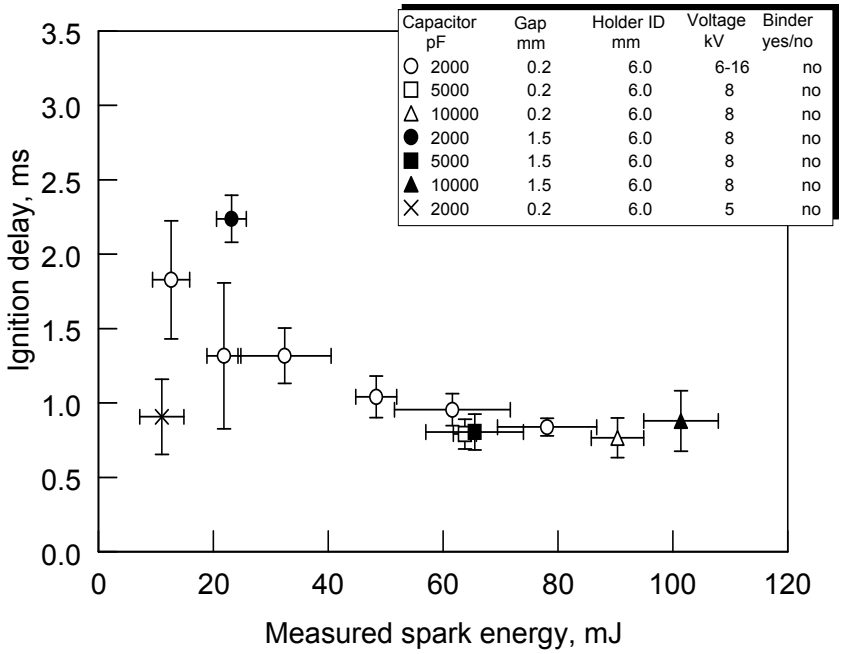

Figure 14. Ignition delay (method 2) v measured spark energy for experiments conducted with the 6 mm diameter sample holder and no binder.

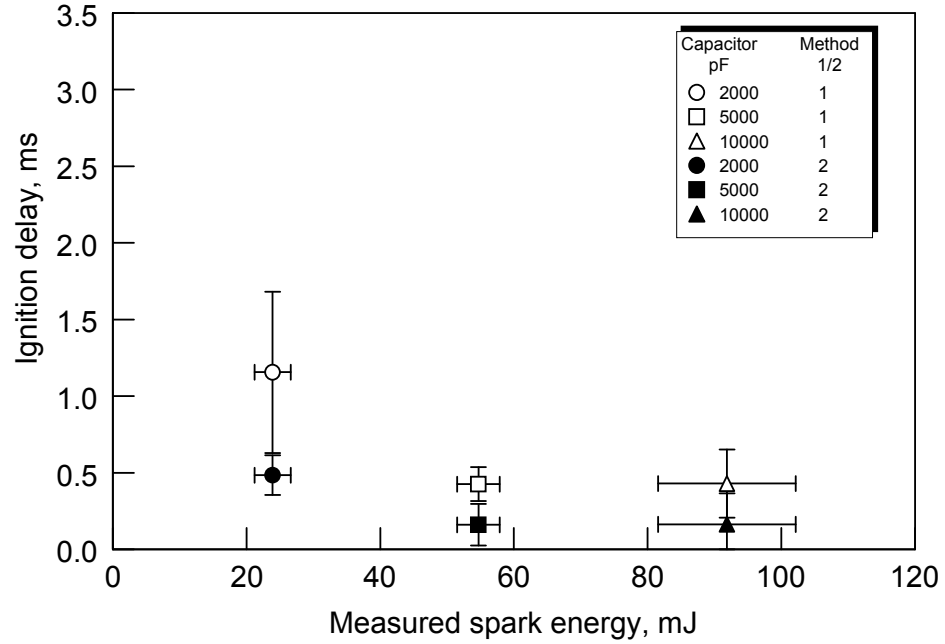

Figure 15. Ignition delay (both methods) v measured spark energy for experiments conducted with the 2.1 mm diameter sample holder and no binder at 8 kV and a gap of 0.2 mm.

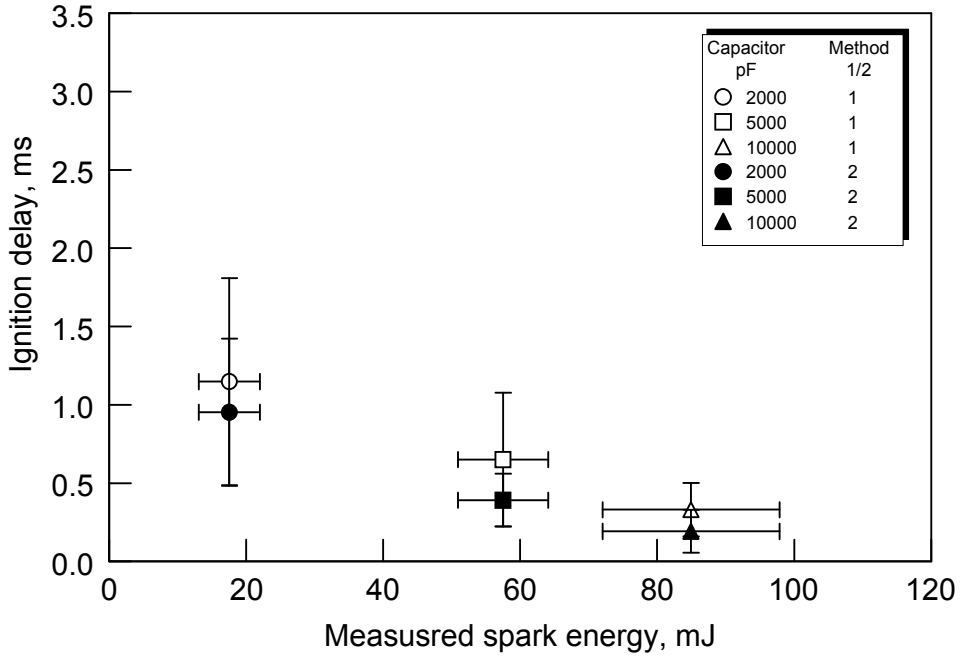

Figure 16. Ignition delay (both methods) v measured spark energy for experiments conducted with the 6 mm diameter sample holder and binder at 8 kV and a gap of 0.2 mm.

DISCUSSION

Spark impedance and measured spark energy

The values of inductance on the order of a few μH are consistent with the measurements reported in [28] for a similar spark configuration. The relatively large additional capacitance values in Figs. 6-8 are clearly not affected by powder or powder/binder mixtures. The additional capacitance values are mostly likely associated with deviations of the capacitor characteristics from their nominal values, stray capacitances produced by the contact between the aluminum substrate and sample holder support, and parasitic capacitance of the output circuit of the FTS. The effect of stray capacitance is further supported considering that the two custom sample holders used different sized aluminum substrates with different contact areas were characterized with consistently different capacitance corrections in experiments.

The resistance values recovered from the current versus time curve fitting for the experiments performed with and without Mg powder can be used to assess the powder electrical resistance. Knowing the current and resistance of the powder enables us to quantify the Joule heating of the powder. Thus, the role of Joule heating in the powder spark ignition mechanism can be clarified. The powder resistance, R_p, was estimated as:

$$R_p = R_w - R_{w/o} \tag{3}$$

where R_w is the circuit resistance obtained for the experiment with powder in the sample holder (cf. Fig. 9), and $R_{w/o}$ is the circuit resistance obtained for the identical capacitance, voltage, and spark gap and using an empty sample holder (cf. Fig. 8). The energy transferred to the powder as a result of its Joule heating is then determined as:

$$E_{Joule} = \sum I^2 R_p \Delta t \tag{4}$$

This processing was performed for each ignition experiment and Fig. 17 shows the result. In addition, the spark total energy for the same conditions obtained using Eq. (2) is also shown for reference. For the experiments with no binder used, the Joule heating energy varies from 50 to 90 % of the total measured spark energy. For the experiments with binder, the values of Joule heating energy and the total spark energy are approximately the same. This discrepancy likely points out at an inaccuracy in quantifying the powder resistance for cases when the binder was used.

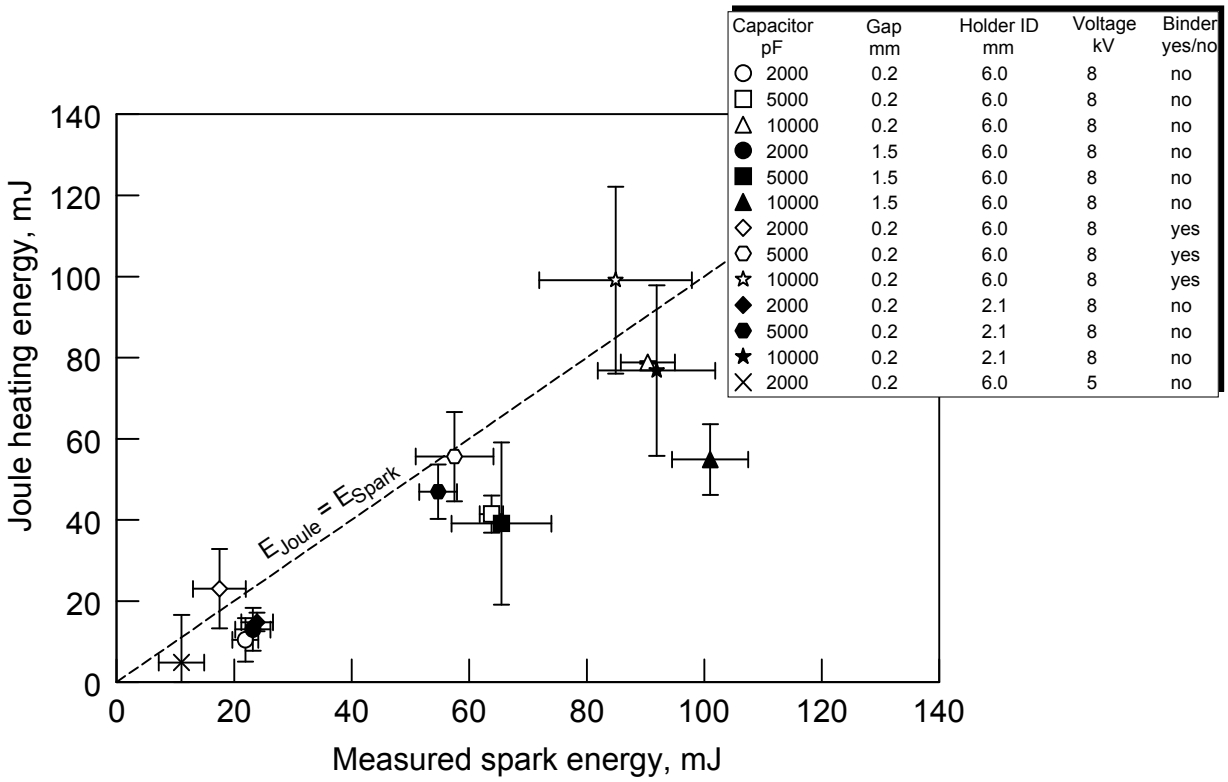

Figure 17. Joule heating v measured spark energy.

The energy transferred to the powder as a result of its Joule heating is substantial and must result in its significant heating. The role of this heating in triggering powder ignition is further discussed below.

Powder heating and ignition by the spark

Spark discharge breaks down the gas gap producing a relatively narrow (~ 100 μm diameter [27, 29]) plasma channel with a small resistance. When an empty sample holder is used, this channel is reaching the metal surface with electrical resistance negligible compared to that of the plasma. However, when metal powder is placed in the sample holder, its electrical resistance is much greater than that of a bulk metal because of the substantial contact resistance between adjacent particles. Thus, in order to achieve comparable currents in both cases, the spark plasma must be extended through the powder layer. In other words, local micro-discharges occur between particles placed under the plasma channel, effectively reducing the contact resistance between these particles. The local discharges between the particles serve as hot spots heating the powder during the spark discharge, while the resistance of the individual particles is much smaller so that their Joule heating by the current existing inside the particles is negligible.

Assuming that the spark discharge directly heats only the powder layer directly under the plasma channel, both diameter, D, and initial temperature, T_{in} of the directly heated powder cylinder can be estimated. This estimate will use the experimentally determined minimum ignition energy for the spark ignition of Mg powder.

First, note that the distance the heat can travel within the powder during the spark duration is negligible. Indeed, using the thermal diffusivity for a Mg powder layer measured in ref. [20], $\alpha = 2.29 \times 10^{-7}\, m^2/s$, it can be readily estimated that in τ = 1 μs (characteristic spark duration) the heat can only travel within the powder for about $\sqrt{\alpha\tau} \approx 0.5$ μm. Thus, for a crude estimate it can be assumed that the powder cylinder of a fixed diameter, *D*, is heated adiabatically and uniformly by the current passing through it. The height of the cylinder, *H*, is taken to be 0.5 mm, which is close to the height of the powder sample placed in the sample holder. For such a cylinder, the temperature achieved as a result of its Joule heating will be a function of the cylinder radius, *R*, as expressed by Eq. (5):

$$\begin{aligned} &if\ T_{in} < T_m; \quad T_{in} = T_0 + \frac{E_{Joule}}{\pi\rho\eta C_{PS} R^2 H} \\ &if\ T_{in} > T_m; \quad T_{in} = T_m + \frac{E_{Joule}}{\pi\rho\eta C_{PL} R^2 H} - \frac{C_{PS}}{C_{PL}}\left(T_m - T_0\right) - \frac{L}{C_{PL}} \end{aligned} \tag{5}$$

where T_0 is the initial powder temperature assumed to be equal to the room temperature, 298 K, T_m=923 K is the magnesium melting temperature, η is packing density, and for densely packed spheres η=0.75, C_{PS} and C_{PL} are the values of specific heat for solid and liquid magnesium respectively, *L*=357.9 kJ/kg, is the latent heat of melting for magnesium, E_{Joule} is the spark energy released in the powder as a result of its Joule heating, and ρ is the powder density. Assuming that E_{Joule}= 5 mJ corresponding to the experimentally determined minimum ignition energy, the temperature, T_{in}, predicted to be achieved in the heated volume is plotted as a function of the cylinder radius (the horizontal axis shown at the top of the plot) in Fig. 18.

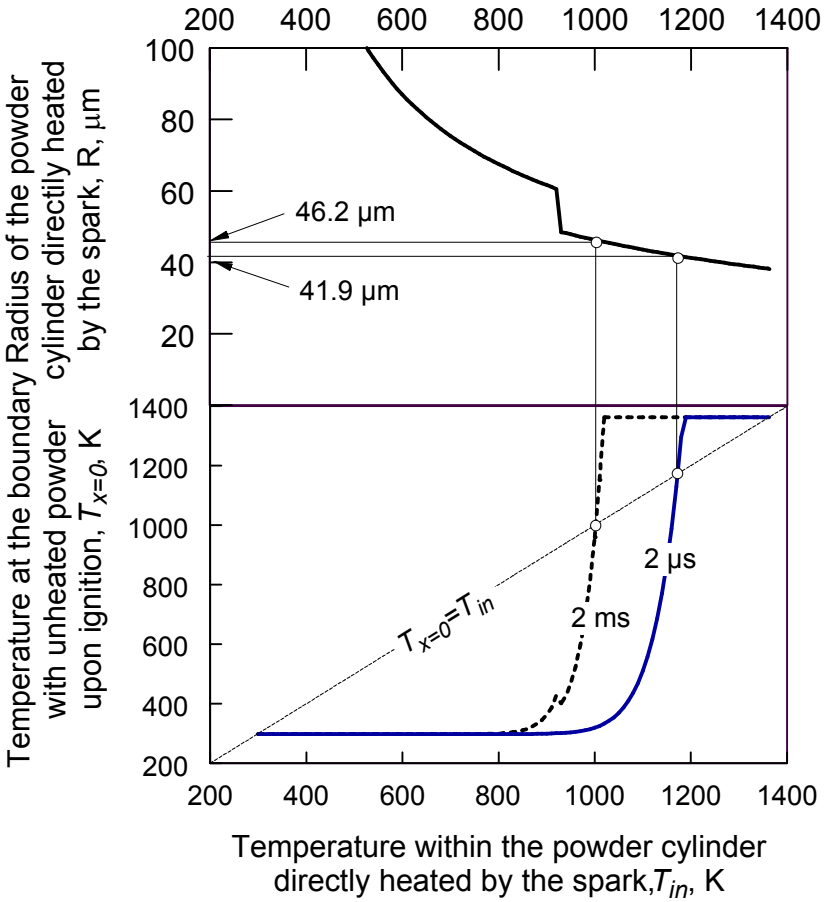

Figure 18. Illustration for evaluation of the radius of the powder cylinder directly heated by the spark. The top plot shows how this radius changes depending on the temperature achieved in the cylinder and assuming that the spark energy is equal to the minimum ignition energy for Mg. The bottom curves show temperatures at the boundary with the cold portion of the powder required to remove the heat generated by chemical reaction within the directly heated cylinder for the time delays of 2 μs and 2 ms.

In order to determine which diameter corresponds to the experimental situation, two separate estimates can be made. In the first case, consider the heat balance between the powder heated by the discharge directly and the rest of the sample, assuming that the powder remains in the sample holder (i.e., neglecting powder ejection). The powder heated by the spark directly will start oxidizing and heat the rest of the sample. Assuming that the oxygen is available to the powder directly heated by the spark (after some ignition delay), the respective heat flux can be described as

$$q_s'' = \frac{A}{A_v} Z \Delta H \exp\left(-\frac{E_A}{R_u T_{in}}\right) = \frac{3R\eta}{2r} Z \Delta H \exp\left(-\frac{E_A}{R_u T_{in}}\right) \quad (6)$$

where A is the area over which oxidation occurs equal to the total surface area of all the particles inside the directly heated cylinder and A_v is the surface area of the heated cylinder in contact with the rest of the surrounding powder; it is assumed that all particles have the same radius, r, equal to the mean radius of the powder used in experiments (5.15

μm), Z is the pre-exponent, ΔH is the enthalpy of oxidation, E_A is the activation energy, R_u is the universal gas constant. The values of $Z=10^{10}$ kg/m^2 s and E_A=215 kJ/mol are taken from ref. [20] where the same Mg powder was studied. For powder ignition to occur, this heat flux needs to be balanced by the heat flux produced in the conductive colder powder outside of the directly heated volume. For a simple estimate, the transient temperature profile in that portion of the sample, T_x as a function of, x, the distance from the interface with the directly heated volume, can be approximately described by an analytical expression available for a semi-infinite solid heated at its boundary by a constant heat flux [30]. For x=0, the heat flux can be expressed through temperature at the interface, $T_{x=0}$ as:

$$q_s^{"} = \frac{2}{k} \cdot \frac{\sqrt{\alpha t / \pi}}{T_{x=0} - T_0} \tag{7}$$

where α is thermal diffusivity, k is thermal conductivity, and t is elapsed time. The value of $q_s^{"}$ can be taken as a function of temperature from Eq. (6), so the radius R of the directly heated cylinder can be found, for which the condition (8) below is satisfied:

$$T_{x=0} = T_{in}(R) \tag{8}$$

The elapsed time is assumed to be equal to the characteristic ignition delay, t=2 ms. For this time, the condition (8) is fulfilled for R=46.2 μm. This calculation is illustrated in Fig. 18. Another borderline case, with the elapsed time close to the spark duration, t=2 μs is also considered.

The simple estimates above can be used to assess the radius of the powder cylinder directly heated by the spark. Based on results presented in Fig. 18, this radius is limited by 41.9 and 46.2 μm. This size compares well with the reported dimension of the plasma kernel produced in similar spark discharges [27, 29].

The second approach for estimating the size of the powder cylinder directly heated by the spark can be considered assuming that the powder is ejected by the discharge, so that observed ignition is effectively equivalent to combustion of the individual ejected particles. To determine to what temperature the particle needs to be heated prior to its ejection so that it will ignite when exposed to cold air, a heat transfer balance between chemical reaction heat release and convective and radiative heat losses can be considered for an individual particle:

$$Z\Delta H \exp\left(-\frac{E_A}{RT_{Particle}}\right) = \frac{Nu}{D} k\left(T_{Particle} - T_\infty\right) + \varepsilon\sigma\left(T_{Particle}^4 - T_\infty^4\right) \tag{9}$$

where $T_{Particle}$ is the temperature of the particle that needs to be reached in order for ignition to occur, Nu is the Nusselt number, D is the particle diameter, k is the thermal conductivity of air taken at the film temperature, T_∞ is the temperature of the surrounding air and surfaces, ε is the emissivity of the particle surface, and σ is the Stefan-Boltzmann constant. The particle is assumed to have a low Reynolds number and therefore the value of $Nu=2$ is used corresponding to a stationary sphere. The temperature at which Eq. (9) is satisfied is assumed to be the ignition temperature for a single Mg particle in cold air. Using the heat balance (9) it is estimated that for a particle of 10.3 μm diameter (the mean diameter of the Mg powder used in experiment) the ignition temperature is 1067 K. From the top curve shown in Fig. 18, this temperature corresponds to the radius of the

heated powder cylinder of approximately 45 μm, which is very close to the previous estimate.

Assuming that this dimension does not change significantly as a function of the spark energy, the ignition delays for different spark energies can be evaluated. It is generally clear that shorter delays will be predicted to correspond to the greater spark energies, as observed experimentally. However, the simple estimates are limited because once the powder in the volume directly heated by the spark starts boiling, the regime of heat transfer between this boiling powder and the colder external portion of the sample change substantially. It also is clear that the description of the oxygen transfer to the heated powder is of critical importance since this transport will determine the rate of reaction in the powder cylinder directly heated by the spark, which, in turn, will likely determine the observed ignition delay. By using Eq. (6) it was assumed that oxygen is available to the powder, while this may not be the case immediately after the spark is over. Indeed, the oxygen available for reaction is contained inside the porous powder layer. An estimate shows that if all this oxygen is consumed, the powder temperature can only be increased by about 2 K. Additional oxygen is therefore required and must be supplied by diffusion and/or convection flux which is likely established during the observed ignition delay.

Effect of powder ejection

Based on the observed velocities of the ejected particles, it can be concluded that the powder effectively remains in place during the spark. The particle velocities do not exceed 1 m/s, so the particles do not move more than 1 μm during the 1 μs long spark discharge. On the other hand, the particles do get displaced during the time comparable to the typical ignition delay. The displacement is of the order of 0.5 – 1 mm, which is close to the height of the sample. The powder ejection during the ignition delay affects the heat transfer between the powder heated by the spark directly and the rest of the sample. It can be generally expected that the heat transfer becomes less efficient when part of the directly heated powder is removed, resulting in longer ignition delays. This effect is qualitatively consistent with the results presented in Figs. 14 and 16: shorter delays are observed for the powder with binder. Also, the delays at higher spark energies and no binder do not decrease with further increase in the spark energy, indicating that the powder removal due to ejection impedes the heat transfer within the powder more significantly.

CONCLUSIONS

It was found that for the characteristic ESD ignition testing configurations, the spark duration is of the order of a few μs. The current in the discharge has substantial AC component so that the polarity of the electrodes was observed to be insignificant for the spark energy transfer to the powder. It was also found that only about 1/3 of the energy stored in the capacitor is supplied to the igniting powder as a result of its Joule heating. For Mg powder used in the experiments, the powder ignition was observed to be delayed by 0.5 – 3.5 ms after the spark discharge is over. Shorter ignition delays were observed for greater spark energies. Portion of the powder was observed to be ejected by the spark

independently whether ignition was or was not observed. It was hypothesized that the ejection is due to a shock wave produced by the spark and reflected from the bottom of the sample holder. Limiting the powder ejection by adding a small amount of binder to the powder affects the dependency of the ignition delay on the spark energy. For the powder with the binder, the decrease in the ignition delays is almost linear as a function of the spark energy. With no binder, the ignition delays level out for the spark energy of about 60 mJ and do not decrease at greater spark energies. A simplified estimate shows that the ignition can be described considering that the spark first adiabatically heats a powder cylinder located directly under the spark plasma channel. Considering the experimentally determined minimum ignition energy for magnesium powder, the radius of this cylinder directly heated by the spark is estimated to be between 42 and 46 μm. This directly heated powder cylinder then starts oxidizing and the released enthalpy of oxidation heats the rest of the powder causing its subsequent ignition.

ACKNOWLEDGEMENT

This work was supported by Dr. Ralph A. Anthenien of the U.S. Army Research Office.

REFERENCES

[1]Mellor, A. M., Stoops, D. R., "Optimization of spark and ESD propellant sensitivity tests, "*Propellants, Explosives, Pyrotechnics,* 15, 1990, pp. 1-7

[2]Mellor, A. M., Baker, P. J., "Propellant properties conducive to electrostatic discharge ignition," *Journal of Energetic Materials,* 12:1, 1994, pp. 1-62

[3]Ryzhik, A. B., "Critical conditions of the spark ignition of metal power suspensions in gas," *Fiz. Goreniya Vzryva,* 14, 1978, pp. 53-57

[4]Ryzhik, A. B., Makhin, V. S., Kititsa, V. N., Il'in, V. V., "Experimental study of the spark ignition of aerosol suspensions of lightweight metal powder, *Tr. Vses. N.-i.i Proekt.In-t Alyum., Magn.i Elektrod.Prom-sti.,* 1977, pp. 106-112

[5]Kim, S. W., Colver, G. M., "Spark ignition of aluminum powder in mixtures of oxygen, nitrogen, and carbon dioxide - a new testing method," *American Society of Mechanical Engineers, Heat Transfer Division,* 148, 1990, pp. 97-104

[6]Kao, C. S., Duh, Y. S., "Accident investigation of an ABS plant," *Journal of Loss Prevention in the Process Industries,* 15 (3), 2002, pp. 223-232

[7]Glor, M., "Hazards due to electrostatic charging of powders," *Journal of Electrostatics,* 16 (2-3), 1985, pp. 175-191

[8]Wu, Z., Chen, Y., Hu, X., Liu, S., "Research on ESD hazards of textiles," *Journal of Electrostatics,* 57, 2003, pp. 203-207

[9]Tunnicliffe, G., Thomson, M., "Explosion protection," *Cleanroom* Technology, 9 (9), 2003, pp. 29-32

[10]Senecal, J. A., "Manganese mill dust explosion," *Journal of Energetic Materials,* 4, 1991, pp. 332-337

[11]Matsuda, T., Yamaguma, M., "Tantalum dust deflagration in a bag filter dust-collecting device," *Journal of Hazardous Materials,* 77 (1-3), 2000, pp. 33-42

[12]Ebadat, V., Pilkington, G., "Dust explosion hazards," *Chemical Processes* 58 (9), 1995, pp. 5

[13]Zeman, S., Kočí, J., "Electric spark sensitivity of polynitro compounds: Part IV. A relation to thermal decomposition parameters," *Journal of Energetic Materials*, 8 (1), 2000, pp. 23-26

[14]Skinner, D., Olson, D., Block-Bolton, A., "Electrostatic discharge ignition of energetic materials," *Propellants, Explosives, Pyrotechnics,* 23, 1997, pp. 23-42

[15]Matsugi, K., Hatayama, T., Yanagisawa, O., "Effect of direct current pulse discharge on specific resistivity of copper and iron powder compacts," *Journal of the Japan Institute of Metals,* 59 (7), 1995, pp. 740-745

[16]Belyaev, A. A., Gutso, D. E., Kiseev, V. M., "Formation of interparticle contact resistance in powder materials," *Poroshkovaya Metallurgiya,* 10, 1992, pp. 83-86

[17]MIL-STD-1751A, Manual of Data Requirements and Tests for the Qualification of Explosive Materials for Military Use, AOP-7, 2003

[18]Electromagnetic compatibility (EMC) - Part 4-2: Testing and measurement techniques - Electrostatic discharge immunity tests IEC 61000-4-2 Edition: 1.2 International Electrotechnical Commission, 2001

[19]Roberts, T. A., Burton, R. L., Krier, H., "Ignition and combustion of aluminum/magnesium alloy particles in O2 at high pressures," *Combustion and Flame,* 92 (1-2), 1993, pp. 125-143

[20]Ward, T. S., Trunov, M. A., Schoenitz, M., Dreizin, E. L., "Experimental methodology and heat transfer model for identification of ignition kinetics of powdered fuels," *International Journal of Heat and Mass Transfer,* 49 (25-26), 2006, pp. 4943-4954

[21]Star Brite liquid electrical tape MSDS, Star Brite product catalog, available at: http://www.starbrite.com/msdssheets/84104%20msds%202-29-08.pdf.

[22]Pearse, R. W. B., Gaydon, A. G., The Identification of Molecular Spectra 4th ed., Chapman and Hall, London, UK, 1976, pp. 209-211

[23]Atomic Spectra Peaks, NIST Atomic Spectra Database v3, available at: http://physics.nist.gov/PhysRefData/ASD/index.html.

[24]Borghese, A., D'Alessio, A., Diana, M., Veintozzi, C., "Development of hot nitrogen kernel produced by a very fast spark discharge," *Twenty-Second Symposium on Combustion/The Combustion Institute*, 1998, pp. 1651-1659

[25]Kerchner, R. M., Corcoran, G. F., Alternating Current Circuits 4th ed., John Wiley & Sons, New York, 1960, pp. 571-572

[26]Sher, E., Ben-Ya'ish, J., Kravichik, T., "On the birth of spark channels," *Combustion and Flame*, 89, 1992, pp. 186-194

[27]Howatson, A. M., An introduction to gas discharges, Pergamon Press, Oxford, 1965, pp. 47-100

[28]McCahill, M. J., Lee, R. J., Remmers, D. L., "Electrostatic Discharge Sensitivity Testing Revisited," JANNAF

[29]Ono, R., Masahuru, N., Fujiwara, S., Horiguchi, S., Oda, T., "Gas temperature of capacitance spark discharge in air," *Journal of Applied Physics*, 97, 2005, pp. 123307, 1-7

[30]Incropera, F. P., Dewitt, D. P., Bergman, T. L., Lavine, A. S., Introduction of Heat Transfer 5th ed., John Wiley & Sons, New York, 2007, pp. 286-292.